JACS
JOURNAL OF THE AMERICAN CHEMICAL SOCIETY

ARTICLE

pubs.acs.org/JACS

Simultaneous Determination of the Adsorption Constant and the Photoinduced Electron Transfer Rate for a Cds Quantum Dot−Viologen Complex

Adam J. Morris-Cohen, Matthew T. Frederick, Laura C. Cass, and Emily A. Weiss*

Department of Chemistry, Northwestern University, 2145 Sheridan Road, Evanston, Illinois 60208-3113, United States

Supporting Information

ABSTRACT: Transient absorption (TA) spectroscopy of solution-phase mixtures of colloidal CdS quantum dots (QDs) with acid-derivatized viologen molecules, *N*-[1-heptyl],*N*′-[3-carboxypropyl]-4,4′-bipyridinium dihexafluorophosphate (V^{2+}), indicates electron transfer occurs from the conduction band of the QD to the LUMO of V^{2+} after photoexcitation of a band-edge exciton in the QD. Analysis of the magnitude of the ground state bleach of the QD as a function of the molar ratio QD:V^{2+} yields the QD−ligand adsorption constant, K_a (4.4×10^4 M^{-1}) for V^{2+} ligands adsorbed in geometries conducive to electron transfer. The value of K_a, together with the measured rates of (i) formation of the $V^{+\bullet}$ electron transfer product and (ii) recovery of the ground state bleach of the QD, enables determination of the *intrinsic* rate constant for charge separation, $k_{CS,int} \sim 1.7 \times 10^{10}$ s^{-1}, the rate for a single QD−V^{2+} donor−acceptor pair. This analysis confirms previous reports that the number of ligands adsorbed to each QD is well-described by a Poisson distribution. This is the first report where the QD−ligand charge transfer and binding equilibria are quantitatively investigated simultaneously with a single technique.

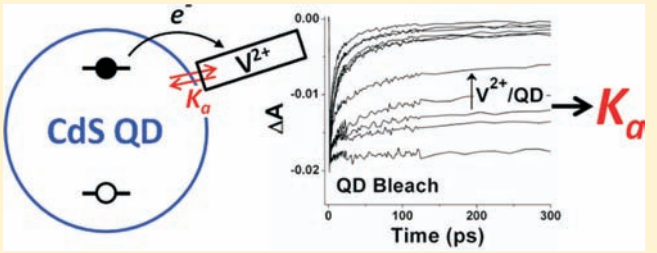

INTRODUCTION

This paper describes a transient absorption (TA) study of photoinduced electron transfer (PET) within colloidal CdS quantum dot−viologen (QD−V^{2+}) complexes. We outline a method to use a single TA experiment to (i) quantitatively determine the average number of ligands adsorbed in geometries that permit electron transfer ("PET-active geometries") per QD at equilibrium (we denote this quantity λ) and (ii) identify the *intrinsic* rate constant for PET, $k_{CS,int}$, the charge separation (CS) rate constant for a single QD−V^{2+} donor−acceptor pair. We determine λ and $k_{CS,int}$ by simultaneously measuring the rate of formation of the $V^{+\bullet}$ radical cation and the magnitude of the recovery of the ground state bleach in the TA spectrum of the QDs upon PET from the conduction band of photoexcited CdS QDs (radii = 1.9−2.3 nm) to the viologen derivative *N*-[1-heptyl],*N*′-[3-carboxypropyl]-4,4′-bipyridinium dihexafluorophosphate (Chart 1). Other groups have observed PET between QDs and various organic molecules,[1−11] organometallic complexes,[12] and TiO_2 nanoparticles,[13−19] but little progress has been made in mapping the structural and chemical parameters of the QD−surfactant interface to the PET rate, or in developing a mechanistic understanding of this heterogeneous PET process. One difficulty in studying PET dynamics in QD−ligand systems is that the PET rate constant observed when multiple redox-active ligands are bound to each QD includes a statistical factor due to the presence of multiple PET pathways.[1,2] It is therefore necessary to isolate the influence of interfacial structure on $k_{CS,int}$ from its influence on this statistical factor in order to interpret the observed PET rate, $k_{CS,obs}$. Knowing the average number of ligands adsorbed per QD in PET-active geometries permits the measurement of $k_{CS,int}$ and thus enables the study of PET dynamics as a function of various interfacial properties.

In addition to facilitating the determination of $k_{CS,int}$, measurement of λ through analysis of the ground state bleach of the QD allows us to calculate an adsorption constant, K_a, for the QD−V^{2+} system; this analysis is therefore a means to compare the adsorption strengths of ligand headgroups, when the headgroups are bound to redox-active moieties that act as a probe of the adsorption event. Not every adsorption event necessarily produces a PET-active QD−ligand configuration, so the value of K_a we derive from this analysis may not equal the value obtained from, for example, NMR, in which chemical shifts of the ligands may be sensitive to formation of non-PET-active QD−ligand complexes.[20] Our TA-based method is therefore complementary to other methods for measuring K_a; however, because the signal we use to measure K_a with TA arises directly and only from electron transfer, this signal will always be present in exactly the systems one wants to study for PET, and is the *only* value of K_a that allows us to calculate $k_{CS,int}$ (methods not specifically sensitive to PET-active configurations would yield artificially high values of K_a for this purpose). Furthermore, the method we present for measuring K_a has several

Received: February 1, 2011
Published: May 27, 2011

dx.doi.org/10.1021/ja2010237 | *J. Am. Chem. Soc.* 2011, 133, 10146–10154

Chart 1. *N*-[1-Heptyl],*N*′-[3-carboxypropyl]-4,4′-bipyridinium (V^{2+})

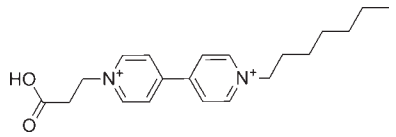

distinct advantages over other types of measurements of equilibrium adsorption constants for QD−ligand systems: (i) Unlike NMR[21−24] and IR, our method uses spectroscopic signals from the QD, not the ligand, to determine the number of bound ligands; we can therefore use low concentrations of ligands (as few as one ligand per QD, a 2 μM solution of ligands in this study) to measure K_a. (ii) Also distinct from NMR and IR, our method for measuring K_a does not rely on small changes in signals from ligands upon association with the QDs; often signals from bound ligands are obscured by much larger, overlapping signals from free ligands. (iii) Unlike ICP and XPS,[25−27] our method does not disrupt the equilibrium between QD and ligand upon measurement of bound ligands, so we get a true measurement of K_a.

One strategy for estimating $k_{CS,int}$ without measuring K_a for a particular QD-ligand system is to prepare samples of QD−ligand complexes in a solvent in which the QD is soluble but the ligand is insoluble, and assume that all ligands in the dispersion are bound to the QDs.[1] This strategy, however, severely restricts the solvent systems and the QD/ligand combinations available to study. Our method not only circumvents the independent measurement of K_a but also accommodates any solvent system in which the QD and ligand can achieve equilibrium.

Previous analyses of electron transfer[2] and energy transfer[28] dynamics in colloidal QD−ligand systems as a function of ligand concentration rely upon variations of the kinetic model developed by Tachiya.[29] In this model, the electron transfer dynamics are described by a sum of exponential functions, where each exponential component corresponds to a population of QDs with a certain number of bound ligands, *n*. The amplitude of a given component corresponds to the fraction of QDs in the sample with *n* bound ligands, and the decay rate of that component is a factor of *n* times the intrinsic rate of electron transfer. Assuming the number of ligands per QD follows a Poisson distribution, the infinite sum of exponentials converges and the resulting function is used to fit the kinetic data. Some variations of this method include terms for relaxation of the excited state of the QD through pathways that compete with the electron transfer process or terms that allow for diffusion of the quenching ligands on or off of the surface of the QD during the lifetime of the excited state. Ultimately, the purpose of this model is to extract both the mean number of adsorbed ligands, λ, and the intrinsic (independent of ligand concentration) rates of relaxation of the excited state of the QD from the relaxation dynamics. Here, we employ the Tachiya model to find the concentration-independent rate of QD-to-ligand PET ($k_{CS,int}$). We find that, for this particular system (CdS−V^{2+}), reducing the number of free parameters in the kinetic fit function (by determining λ from the amplitude of the ground state bleach of the QD as a function of the concentration of free V^{2+} ligand) is necessary to achieve robust and physically meaningful values of $k_{CS,int}$.

Experimental Design. We chose *N*-[1-heptyl],*N*′-[3-carboxypropyl]-4,4′-bipyridinium dihexafluorophosphate (V^{2+}) (Chart 1) as the electron-accepting ligand because the closely related methyl viologen dichloride (MV^{2+}) molecule has a well characterized reduction potential and radical cation ($MV^{+\bullet}$) spectrum, and has been shown to participate in ultrafast (70−1000 fs) electron transfer with colloidal CdS and CdSe QDs under a wide variety of experimental conditions.[30−36] Rapid electron transfer is important in this experiment because we require that PET outcompete relaxation pathways for the photoexcited electron that would prevent ET, such as radiative recombination with the hole, which occurs on the nanosecond time scale. We used the hexafluorophosphate salt of V^{2+} (Chart 1) instead of the commercially available MV^{2+} because we wanted the ligand to be soluble in solvents compatible with the QDs, and because we plan, in future studies, to explore the functional dependence of the PET rate on the ligand's coordination group, linker length, and adsorption geometry. A quantitative analysis of these phenomena requires a technique to measure λ and $k_{CS,int}$ for a series of viologen derivatives; this paper describes that technique.

EXPERIMENTAL METHODS

Synthesis of *N*-[1-heptyl],*N*′-[3-carboxypropyl]-4,4′-bipyridinium dihexafluorophosphate (V^{2+}). All reagents were purchased from Sigma Aldrich and used as received. We synthesized V^{2+}, Chart 1, using a modified literature procedure.[37] Adding 0.420 g of 1-heptyl-4-(4-pyridyl)pyridinium bromide and 0.680 g of ethyl-3-bromopropionate to 10 mL of acetonitrile (ACN) and refluxing with stirring under a nitrogen atmosphere for 3 days produced a yellow suspension. We filtered and washed the suspension with three 10 mL portions of diethylether (Et_2O) and then dissolved it in 2 mL of 2 M HBr. After 3 days under open atmosphere, the HBr solution was evaporated leaving a viscous brown liquid. Adding 10 mL of Et_2O to the remaining brown liquid produced a yellow suspension. We filtered the yellow precipitate, dissolved it in 5 mL of deionized water, and treated the solution dropwise with a concentrated solution of ammonium hexafluorophosphate. The resulting white precipitate was filtered and washed with 10 mL of deionized water and dried under vacuum. ^{1}H NMR (methanol, 500 MHz, ppm): 9.22 (d, 2H, 6.83 Hz), 9.16 (d, 2H, 6.84 Hz), 8.54 (m, 4H), 4.92 (t, 2H, 6.2 Hz), 4.67 (t, 2H, 7.81 Hz), 3.13 (t, 2H, 6.1 Hz), 2.3 (m, 2H), 1.37 (m, 4H), 1.28 (m, 4H), 0.85 (t, 3 Hz, 6.83 Hz). MALDI: 327.8 *m*/*z*.

Synthesis and Purification of CdS Quantum Dots. We synthesized CdS QDs by first adding 90% technical grade oleic acid (1 mL, 3.2 mmol), 90% technical grade octadecene (4.9 mL, 15.3 mmol), and cadmium oxide (0.0128 g, 0.1 mmol) to a dry, three-neck round-bottom flask. We heated the reaction mixture to 300 °C under a N_2 atmosphere and stirred vigorously. Once the solution became clear, we injected elemental sulfur (0.0016 g, 0.05 mmol) dissolved in 1 mL of octadecene and allowed the QDs to grow at 300 °C. In order to extract the unused cadmium precursor, an equal volume of 1:1 $CH_3OH/CHCl_3$ was added to the QD colloidal suspension. This mixture was centrifuged at 3500 rpm for 5 min. The cadmium precursor separated into the bottom $CH_3OH/CHCl_3$ layer, while the QDs remained in the top layer of octadecene. We decanted this top layer and precipitated the QDs by the addition of acetone and centrifugation. We then discarded the supernatant, redispersed the QDs in CH_2Cl_2 (DCM), and filtered this final solution using 0.45 μm syringe filters to remove any remaining aggregates.

Preparation of Samples for Transient Absorption (TA). To ensure that the TA results were reproducible and general from batch to batch, we repeated the TA measurements on three different batches of CdS QDs synthesized on three different days, each with a series of V^{2+}/QD molar ratios: 0, 1, 2, 4, 8, 10, (12 or 16), (20 or 24), 30, 40, 50, 60, and 70 V^{2+} molecules added per QD. We prepared the TA samples by adding a stock solution of V^{2+} in ACN at the appropriate concentration

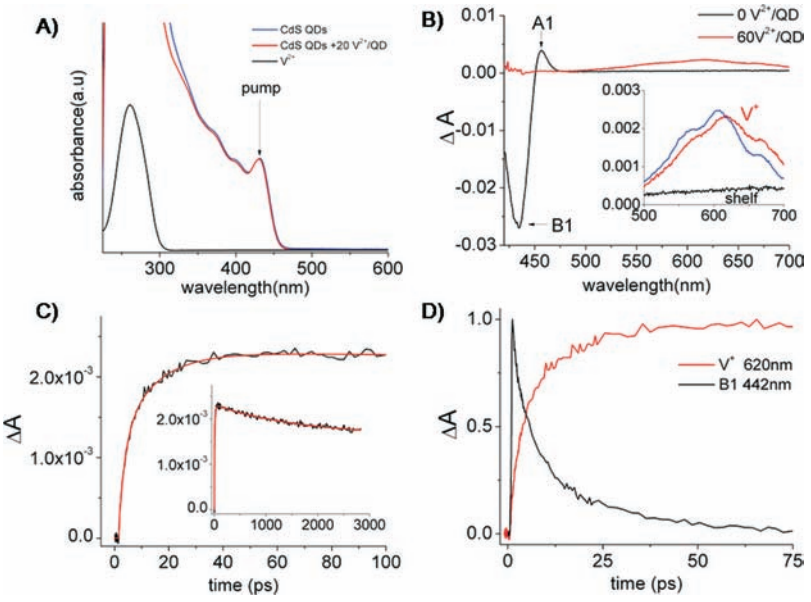

Figure 1. (A) Ground state absorption spectrum of V^{2+} (black) and of QDs (radius = 2.3 nm) without added V^{2+} (blue) and with V^{2+} added in a molar ratio of 20:1 V^{2+}/QD (red). The arrow indicates the wavelength of the excitation pump in the TA experiment. (B) TA spectra, 100 ps after photoexcitation, of 2.3-nm, 2.3×10^{-6} M CdS QDs in CH_2Cl_2/ACN without (black) and with (red) 60 V^{2+} added per QD, and comparison with the spectral signature of $V^{+\bullet}$ in steady state spectroelectrochemistry (inset, blue). The B1 feature is quantitatively quenched by PET. The sample without V^{2+} has a flat, but nonzero amplitude from 500 to 700 nm that we term the "shelf". (C) Representative TA kinetic trace at 620 nm, the peak of the $V^{+\bullet}$ absorption, from the TA spectrum of the sample with 60 V^{2+}/QD (shown in (B)). The black line is the experimental data and the red line is a best fit to the data using an IRF convoluted with the sum of four exponential functions, two of which fit the rise of the signal and two of which fit the decay (inset). (D) Normalized kinetic traces of B1 at 442 nm inverted about the *x*-axis (black) and $V^{+\bullet}$ at 620 nm (red) from the same QDs as in (C).

to a stock solution of QDs in CH_2Cl_2. Samples with between 1 and 24 V^{2+} added per QD were in 3% ACN/97% DCM, while samples with between 30 and 70 V^{2+} added per QD were prepared in concentrations of ACN up to 10%. Using different amounts of ACN for the samples with 1−24 V^{2+} ligands per QD and the samples with 30−70 V^{2+} per QD was necessary due to the relative solubilities of V^{2+} and the QDs. The Supporting Information contains data from control experiments that show that changing the amount of ACN in the samples at these concentrations does not change the PET dynamics. We allowed all mixtures to equilibrate for 1−3 days before acquiring their TA spectra.

Transient Absorption Spectroscopy. Our TA setup is described in the Supporting Information and elsewhere.[38] All TA samples had an optical density of 0.3 at the band edge absorption of the QDs. We performed TA measurements on the three batches of QDs on three different days, and for each set of TA experiments we carefully controlled the power, spot size, and sample geometry to ensure that the pump beam created, on average, 0.3 excitons per QD.

Electrochemistry and Spectroelectrochemistry. Cyclic voltammetry (CV) experiments were performed using a Princeton Applied Research VersaSTAT 3 potentiostat, a 3 M Ag/AgCl reference electrode, a Pt counter electrode, and a glassy carbon (apparent area of 28 mm^2) working electrode. The glassy carbon electrode was polished with 0.05 μm alumina powder immediately before use. Spectroelectrochemistry experiments were performed in a 1 mm cuvette with a Pt wire mesh working electrode, Ag/AgCl reference electrode, and Ag counter electrode. All samples were analyzed in ACN degassed with N_2 and kept under an N_2 atmosphere for the duration of the experiment. The supporting electrolyte was 50 mM tetrabutylammonium hexafluorophosphate ($TBAPF_6$).

RESULTS AND DISCUSSION

Characterization of the CdS QDs. Steady state absorption spectra of the three batches of CdS QDs used in this study show a maximum of the band-edge absorbance of 433, 420, and 416 nm corresponding to radii of 2.3, 2.0, and 1.9 nm,[39] respectively. Photoluminescence emission spectra of the samples show an intense, sharp peak Stokes-shifted from the band-edge absorbance by ~11 nm and a broad, weaker peak centered at 600 nm corresponding to deep trap emission. The Supporting Information contains representative absorption and photoluminescence spectra, a transmission electron micrograph, and results from elemental analysis of the CdS QDs.

Transient Absorption Spectra and Dynamics. *The Visible TA Spectra of CdS QDs.* The TA spectra of CdS QDs with their native ligands have three main features (Figure 1): (i) an intense ground state bleach of the band-edge absorption (B1), (ii) a photoinduced absorption (A1) at ~20 nm longer wavelength than B1, and (iii) a broad, low-amplitude photoinduced absorption from 500 to 700 nm that we refer to as the "shelf". The ground state bleach, B1, results from filling the $1S_e$ state with electrons upon photoexcitation of the QDs. The intensity of this signal only reflects the population of electrons in this state; it is not sensitive to the presence of holes in the valence band.[40,41] The A1 feature results from the band-edge absorbance of probe light by QDs that already contain one exciton due to excitation by the pump; the absorbance of the second exciton is shifted to lower energy from the ground state band gap by the exciton−exciton stabilization energy.[42] The shelf has been observed previously in CdSe QDs and assigned to intraband transitions of the excitonic hole because it disappears in the presence of hole scavenging ligands.[2] In our TA spectra of the QDs without added V^{2+}, the shelf consistently forms within 2−6 ps of photoexcitation and has no detectable decay on the time scale of our measurement (3 ns, see Supporting Information).

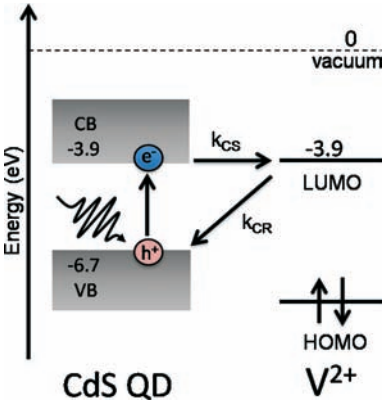

Figure 2. Schematic diagram illustrating the charge separation (CS) and charge recombination (CR) processes that occur after generating a band-edge exciton in the CdS QD. The conduction band (CB) and (valence band, VB) energy levels of the QD are estimated as the CB and (VB) energy levels of bulk CdS plus (minus) half of the difference in optical bandgap between bulk CdS and the QD. The LUMO of V^{2+} is calculated from the reduction wave in the cyclic voltammogram (see the Supporting Information). In this work, we measured the rate of CS as a function of the concentration of V^{2+} adsorbed to the surface of the QD.

Photoexcitation of the QD–V^{2+} Complexes Produces $V^{+\bullet}$. An absorbance centered at 620 nm appears within ~50 ps of photoexcitation of the QD–V^{2+} system at the band-edge absorption of the QD. At this excitation wavelength, only the QDs have measurable absorbance, so we do not create a photoexcited state of V^{2+} (Figure 1A). The TA feature at 620 nm indicates the presence of the $V^{+\bullet}$ radical cation and matches the spectrum we obtain by electrochemically reducing V^{2+} in solution (Figure 1B). Figure 1C shows a representative kinetic trace at 620 nm, plotted over 100 ps to show the rise of the signal and over 3000 ps (the entire time window we monitored) to show the decay of the signal. Concurrent with the appearance of the $V^{+\bullet}$ feature is the recovery of B1 (Figure 1D); the anticorrelation between the amplitude of B1 and the amplitude of $V^{+\bullet}$ suggests that electrons are emptying from the conduction band of the QD into the LUMO of V^{2+} (Figure 2). We can accurately measure the reduction potential of V^{2+}, but we can only estimate the potentials for the QDs (and therefore the driving force, ΔG, for the charge separation reaction) because solution phase CV experiments yield irreversible reduction and oxidation of the QDs (see the Supporting Information for details).[43]

As we will discuss in detail below, both $k_{CS,obs}$ and the magnitude of recovery of B1 depends on the number of V^{2+} molecules, λ, associated with each QD in a PET-active geometry. The charge recombination (CR) process, as detected by the decay of the signal from $V^{+\bullet}$ (Figure 1C, inset), occurs on a time scale longer than we can accurately measure with our optical delay track; we will explore CR dynamics in a separate study.

Global Analysis of the $V^{+\bullet}$ TA Spectrum to Obtain the Observed Charge Separation Rate Constant. The dynamics of the $V^{+\bullet}$ feature centered at 620 nm fit to an instrument response function (IRF) convoluted with a sum of four exponential functions, two that describe the rise of the signal and two that describe the decay (eq 1). In eq 1, $\Delta A(t)$ is the signal intensity at time t

$$\Delta A(t) = \mathrm{erf}\left(\sum_{i=1}^{4} A_i\, e^{-k_i t}\right) \qquad (1)$$

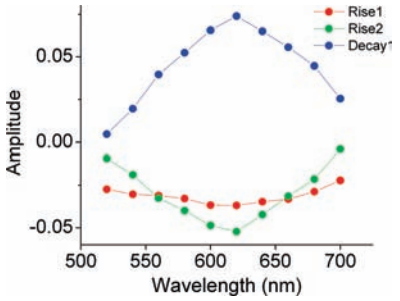

Figure 3. Amplitudes from multiexponential global analysis of the region of the TA spectrum from 520–700 nm; the signal decomposes into a rise (negative amplitude, green) due to formation of $V^{+\bullet}$, a rise (negative amplitude, red) due to formation of the "shelf", and a decay (positive amplitude, blue) due to decay of $V^{+\bullet}$. Not shown is a second component of the decay that was too long to fit accurately, but was required to obtain an adequate fit.

in the TA spectrum, erf is an error function accounting for the instrument response, and the sum of exponentials describes the rise and decay dynamics of the signal with rates $k_i = 1/\tau_i$. Four was the minimum number of exponential functions required to adequately fit the data, that is, to yield a symmetric, random distribution of residuals around the zero line.

For samples with V^{2+}, the faster component of the rise at 620 nm has a time constant of ~3 ps, which is similar to that for the rise of the shelf feature apparent in spectra of QD samples without V^{2+} (2–6 ps, see the Supporting Information). The observed dynamics of the rise at 620 nm therefore result from both the formation of $V^{+\bullet}$ after PET and the formation of the shelf feature. We used a global regression algorithm to decompose the spectrum and dynamics of the feature centered at 620 nm into the contribution of the QD shelf and the contribution of the $V^{+\bullet}$ signal. The general global analysis procedure is described elsewhere.[38] We fit kinetic traces every 20 nm from 520 to 700 nm, a range that roughly spans the $V^{+\bullet}$ absorbance, to eq 1. We constrained these fits such that the fit functions for all wavelengths have the same four time constants, but the amplitudes are allowed to vary from wavelength to wavelength. Figure 3 shows a plot of the amplitudes of each component as a function of wavelength for a sample with two added V^{2+} per QD. Components describing the rise of the signal have negative amplitudes (green, red), and components describing the decay of the signal have positive amplitudes (blue). We do not show amplitudes from the second (longer) component of the decay because it is well beyond our measurable time window. The amplitudes of the slower rise process ("Rise 2", green) and the faster decay process ("Decay 1", blue) reconstruct the spectral shape of the $V^{+\bullet}$ feature shown in Figure 1B, while the amplitudes of the faster rise process ("Rise 1", red) reconstruct the shape of the shelf feature. This analysis strongly implies that Rise 1 (with time constants over the series of samples of ~3 ps) is due to the formation of the shelf and that Rise 2 is due to formation of the $V^{+\bullet}$ cation feature after PET: $k_{rise2} = k_{CS,obs}$. We note that, as the concentration of V^{2+} on the surface of the QD increases and the value of k_{rise2} approaches the value of k_{rise1}, the global analysis no longer effectively separates the two signals (see the Supporting Information). Based, however, on the deconvolution of the signals at low V^{2+} concentration, and the similarity of k_{rise1} to k_{rise} with no added V^{2+}, we believe that k_{rise2} still corresponds to the PET process even at higher concentration of V^{2+}.

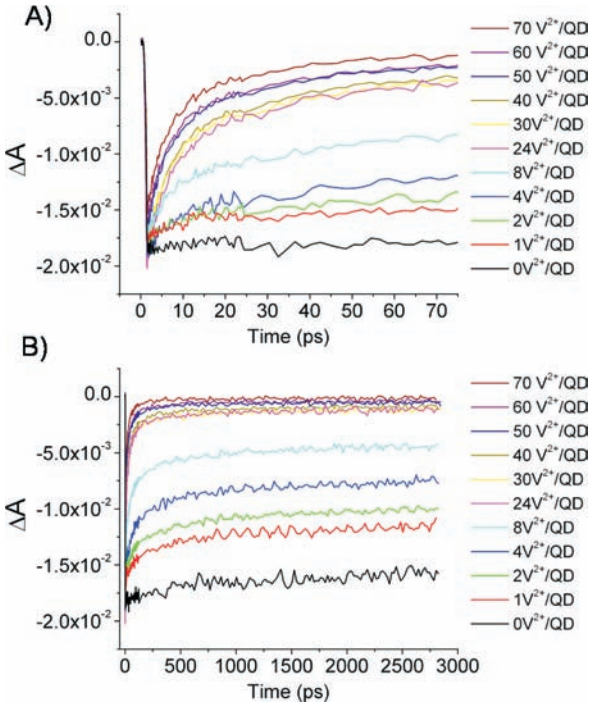

Figure 4. Kinetic traces of the GS bleach of the QDs (B1) at 421 nm, recorded after band-edge excitation of 3.5×10^{-6} M CdS QDs (radius = 1.9 nm) in CH_2Cl_2/ACN, for a series of concentrations of added V^{2+}, from 0 to 75 ps (A), to highlight the dependence of the short-time B1 dynamics on $[V^{2+}]$, and from 0 to 3000 ps (B), to highlight that the long-time (post-PET) B1 dynamics depend only on the decay of the exciton in the free QDs and not on V^{2+}. The Supporting Information contains a plot of the long-time kinetics traces overlaid. The concentration of QDs and pump fluence were kept constant for all of the measurements to enable direct comparison of the amplitudes between traces without normalization.

The value of $k_{CS,obs}$ increases as the concentration of V^{2+} added to the QD dispersions increases (see Supporting Information for a plot of $k_{CS,obs}$ vs added V^{2+} per QD). This result is expected because others have shown that the observed CS rate is proportional to the number of redox-active ligands bound to each QD,[1,2,44,45] eq 2,

$$k_{CS,obs} = nk_{CS,int} \quad (2)$$

where $k_{CS,int}$ (the "intrinsic" PET rate) is the rate of charge separation when each QD has only one redox active ligand adsorbed to its surface and n is the number of ligands adsorbed to the QD. To determine $k_{CS,int}$, we need to find the average value of n in the ensemble; we denote that average value λ ($\lambda = \langle n \rangle$).

Determination of λ by Analysis of the Amplitude of B1. As the concentration of added V^{2+} increases, the degree to which B1 recovers after completion of the PET process increases (Figure 4). We use the degree of recovery of B1 to calculate λ. In order to relate B1 to λ, we assume that (i) any QD with at least one adsorbed V^{2+} will undergo PET, (ii) the B1 feature of any single QD that participates in PET (and therefore no longer has an electron in its conduction band) will recover completely due to the PET, and (iii) the long-time (post-PET) dynamics of the B1 feature are independent of $[V^{2+}]$. Assumption (i) is justified when the PET rate is much greater than the rates of other processes available for electron relaxation. In this system, the

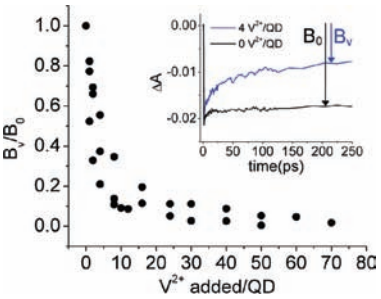

Figure 5. Ratio of the amplitude of the GS bleach of the CdS QDs with added V^{2+} (B_V) to that of the sample with no added V^{2+} (B_0), calculated as described in the text, for all three samples of QDs. The ratio B_V/B_0 is the probability of finding a QD within the ensemble that has zero V^{2+} molecules adsorbed to its surface. Inset: Kinetic traces of B1 at 442 nm recorded after excitation of 2.3×10^{-6} M CdS QDs (radius = 2.3 nm) in DCM/ACN for QDs with 0 added V^{2+}/QD (black) and 4 added V^{2+}/QD (blue). The arrows at 205 ps show one of the delay times at which the amplitudes of B_V and B_0 were monitored to calculate B_V/B_0.

PET lifetime is 10−50 ps and the radiative recombination lifetime is on the order of 10 ns. Electron trapping can also remove electrons from the conduction band; however, in the B1 dynamics of the QD-only sample (no V^{2+}), B1 does not recover on the time scale of the PET reaction.[46,48] Assumption (ii) has been experimentally verified by others[2,40,41] who have shown that the magnitude of B1 depends only on the population of electrons in the lowest-energy conduction band state. We know that assumption (iii) is valid because the kinetic traces of the B1 feature are identical when plotted from 200 to 3000 ns (see the Supporting Information). We can therefore isolate these long-time dynamics from the portion of the dynamics due to the concentration-dependent PET process (i.e., the distributed dynamics) and, as described previously,[45] use the long-time dynamics to assess the total contribution of the concentration-dependent process to the overall recovery of the bleach.

Given these assumptions, the long-time (post-PET) amplitude of B1 decreases because, as more V^{2+} molecules are added to the solution, more QDs within the ensemble have at least one V^{2+} ligand adsorbed to their surface (Figure 4) and undergo PET. Conversely, the more QDs with zero adsorbed V^{2+} ligands, the bigger the amplitude of B1. The ratio of the amplitude of B1 in a sample of QDs with added V^{2+} (B_V) to the amplitude of B1 in a sample of QDs with no added V^{2+} (B_0) at a time when the PET process is complete is equal to the probability of finding a QD in the ensemble with zero adsorbed V^{2+} ligands (Figure 5, inset). We average B_V/B_0 for each sample over a set of times after the completion of the PET process through a procedure that we describe in detail in the Supporting Information. Figure 5 shows B_V/B_0 as a function of the number of V^{2+} added to the QD dispersion for all three samples. We define the detection limit for this technique to be the value of added V^{2+}/QD at which B_V becomes positive, that is, at which the magnitude of B_V is less than the magnitude of the noise in the B1 signal. The data in Figure 5 only include values of B_V/B_0 that lie within this detection limit.

We then assume that the probability of a V^{2+} ligand adsorbing to a QD does not depend on the number of V^{2+} ligands already adsorbed to that QD; this assumption is valid here because the number of ligands (1−70 per QD) is small relative to the number of available surface sites (~350−473 per QD). In the case of

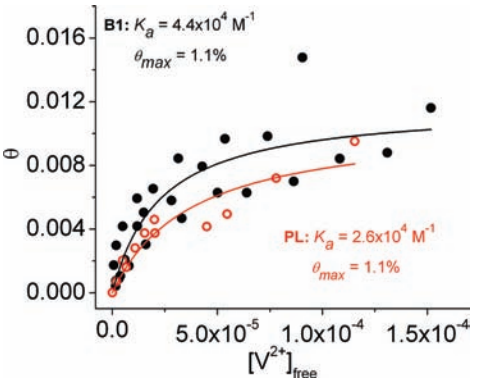

Figure 6. Black: The mean surface coverage, θ (occupied surface sites/total surface sites), of V^{2+} on CdS QDs as a function of the number of unbound V^{2+}, calculated using eq 4 for all three samples of QDs. The Langmuir fit (eq 5) to this data yields the QD−V^{2+} adsorption constant $K_a = 4.4 \times 10^4\ M^{-1}$ and a saturated surface coverage, θ_{max}, of 1.1%. Red: The Langmuir isotherm for a subset (only QDs with radius of 2.0 nm) of the same set of samples, obtained by measuring the magnitude of PL of the QDs as a function of added V^{2+}, as described in the text. The fit of this data to eq 5 yields $K_a = 2.6 \times 10^4\ M^{-1}$ and $\theta_{max} = 1.1\%$.

noninteracting ligands, the number of adsorbed ligands per QD follows a Poisson distribution,[2,28,29] and the probability of finding a QD with n adsorbed ligands, $p(n,\lambda)$, is given by eq 3, where λ is the mean number of ligands adsorbed to the QDs.

$$p(n,\lambda) = \frac{\lambda^n}{n!} e^{-\lambda} \quad (3)$$

We have already defined B_V/B_0 as $p(n,\lambda)$ when $n = 0$, so we can solve eq 3 (with $n = 0$) for λ to yield eq 4.

$$\lambda = -\ln(B_V/B_0) \quad (4)$$

Equation 4 defines the mean number of adsorbed ligands per QD as a function of the number of added ligands, because B_V/B_0 is a function of the number of added ligands (Figure 5).

Calculation of K_a for CdS−V^{2+}. We can convert λ to θ, the mean fractional surface coverage of the QDs by V^{2+}, using the estimated number of available binding sites per QD, n_{sites} (see the Supporting Information). Figure 6 shows an adsorption isotherm: θ versus the concentration of free V^{2+} in the mixture ($[V^{2+}]_{free} = [V^{2+}]_{added} - [V^{2+}]_{adsorbed}$, where $[V^{2+}]_{adsorbed} = \lambda[QD]$). The scatter in this plot results from variation between the three batches of QDs we included in this data set, primarily because these batches are not exactly the same size (Table S1 in the Supporting Information).

We fit the solid symbols to a Langmuir isotherm, eq 5.[47]

$$\frac{\lambda}{n_{sites}} = \theta = \theta_{max} \frac{K_a[V^{2+}]_{free}}{1 + K_a[V^{2+}]_{free}} \quad (5)$$

This fit yields K_a, the adsorption constant for the CdS QD−V^{2+} complex, and θ_{max}, the maximum fractional surface coverage of the V^{2+} molecules on the surface of the QD; we find that $K_a = 4.4 \times 10^4\ M^{-1}$ and $\theta_{max} = 1.1\%$. This value of K_a is within the range of previously measured values of binding constants ($1 \times 10^2 - 1 \times 10^5\ M^{-1}$) for colloidal QD−organic-ligand systems measured using NMR[21−24] and PL.[48] The low value of θ_{max} probably results from high initial coverage of the surfaces of the QDs with their native oleic acid ligands. This result possibly indicates that, as we have suggested previously for weak-binding aniline ligands,[21] the V^{2+} does not displace the native ligands, but rather adsorbs only on patches of the QD surface that are revealed when van der Waals interactions among the alkyl tails of the native ligands cause them to form bundles on the surface of the QDs.

To obtain an independent measurement of K_a and validate our analysis of B1, we measured the photoluminescence (PL) quenching of the QDs as a function of added V^{2+}. Systems like CdS−V^{2+}, in which PET quenches PL faster than any other nonradiative mechanism, are amenable to determination of K_a by PL measurements because we can apply the same logic to the PL response to added V^{2+} as we applied to the B1 response to added V^{2+}: we consider V^{2+} to be a quantitative quencher and define PL/PL_0 (the fraction of PL that remains after addition of V^{2+} at a given QD:V^{2+} ratio) as the fraction of QDs that have zero adsorbed V^{2+}. The fit to the isotherm (θ vs $[V^{2+}]_{free}$) to eq 5 yields $K_a = 2.6 \times 10^4\ M^{-1}$ and $\theta_{max} = 1.1\%$. The PL and TA methods for determining K_a therefore agree within a factor of 2. We note that, for reasons we detail in the Supporting Information, K_a measured by PL (and probably by TA) is dependent on the absolute concentration of the QD−V^{2+} sample; therefore, in order to use the value of K_a measured by PL to facilitate the analysis of the electron transfer rate, one needs to do the PL and TA measurements at the same absolute concentration. This requirement is trivial when using the TA measurement itself to determine K_a, but it is problematic when using PL to determine K_a because TA measurements are normally performed at concentrations 10−50 times higher than used for PL. Here, we used a front-face collection geometry to minimize the contribution of filtering effects associated with measuring PL of samples with optical densities higher than ~0.05, but there is probably error in our PL-determined value of K_a due to reabsorption that we could not eliminate.

Certain assumptions of the Langmuir model (most notably, the assumption of a single physical and electronic structure of the binding sites on the QD surface) in principle decrease the accuracy of this model. Our plot of θ vs $[V^{2+}]_{free}$ fits well to the Langmuir equation, however, so we are not justified in invoking a more complicated model in this case. Our estimation of n_{sites} and our calculation of the concentration of QDs from the published molar absorptivity[42] are potential sources of error in the calculation of K_a, and the Supporting Information contains plots illustrating how these uncertainties propagate into uncertainty in K_a. We attempted to confirm our TA- and PL-derived value of K_a with a ^{1}H NMR-based method that we had used successfully for QD−aniline systems,[21] but we did not observe any signal from V^{2+} (bound or unbound) at the concentrations of QDs and V^{2+} relevant to the TA experiment.

It is difficult to make meaningful comparisons between our value of K_a for V^{2+} and CdS QDs ($4.4 \times 10^4\ M^{-1}$) and those measured for other QD−ligand systems because we do not have any chemical details on how the V^{2+} adsorbs onto the surface of the QD. Taking into consideration the ultrafast CS times between MV^{2+} and CdSe QDs reported by other groups[30−36] the fact that, unlike V^{2+}, MV^{2+} does not contain any functional groups capable of coordinating to the surface of the QD, and the low saturation coverage of V^{2+} on the surface of the QDs, it is possible that the primary driving force for adsorption is the affinity of V^{2+} for the polar surface of the QD and its poor solubility for the primary solvent, CH_2Cl_2. We are currently comparing V^{2+} to other viologen derivatives with various functional groups that should affect the strength of the QD−V^{2+} interaction, so that we can gain a deeper understanding of the nature of the adsorption.

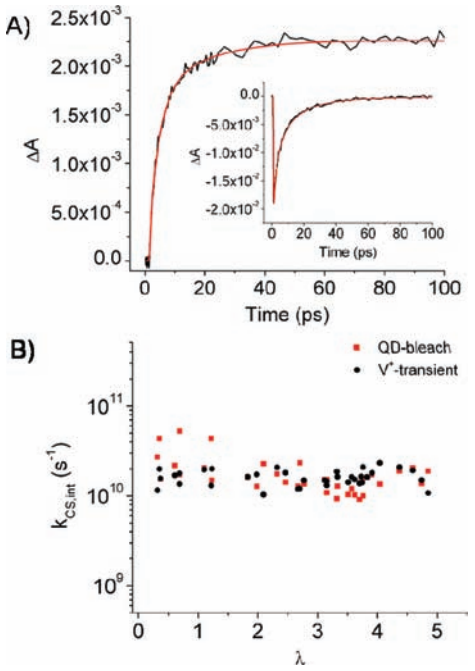

Figure 7. (A) Representative TA kinetic traces at 620 nm, the peak of the $V^{+\bullet}$ absorption, and at 442 nm, the B1 feature (inset), from the TA spectrum of the of 2.3 nm, 2.3×10^{-6} M CdS QDs in CH_2Cl_2/ACN with 60 V^{2+} added per QD. The trace at 620 nm is fit withthe Poisson derived fit function from eq 6 plus three three simple exponential functions to describe the formation of the shelf feature and the decays of $V^{+\bullet}$ and the shelf. The trace at 442 nm is fit with the Poisson-derived function plus four exponential functions (with constraints described in the text). (B) The intrinsic rate of PET, $k_{CS,int}$, extracted from the Poisson-derived fits of the B1 (red) and $V^{+\bullet}$ (black) features, for all of the QD samples as a function of λ. The intrinsic rate of electron transfer, $k_{CS,int}$, averaged over these data, is $1.7 \pm 0.7 \times 10^{10}$ s^{-1}.

Determination of the Intrinsic Rate of PET from the QD to V^{2+}, $k_{CS,int}$. Before finding $k_{CS,int}$ by fitting the dynamics of the $V^{+\bullet}$ radical cation feature and the ground state bleach, we first calculated λ for all samples (including those outside the detection limit of the B_V/B_0 analysis) by solving eq 5 for λ and using our derived value of $K_a = 4.4 \times 10^4$ M^{-1} and $[V^{2+}]_{free} = [V^{2+}]_{added} - \lambda[QDs]$. We use these values of λ to determine $k_{CS,int}$ by fitting the kinetic trace for each QD$-V^{2+}$ sample at 620 nm and at the peak of the B1 feature with the model developed by Tachiya;[29] this model assumes that the number of V^{2+} per QD follows Poisson statistics and that the CS rate for a population of QDs with n adsorbed V^{2+} molecules is $nk_{CS,int}$ (eq 2). We replace the simple exponential function describing Rise 2 for the 620 nm feature (which we determined through global analysis to be the component describing the formation of $V^{+\bullet}$) with the sum of an infinite number of exponential functions, each of which describes the observed CS rate, $nk_{CS,int}$, for a particular population of QDs, eq 6.

$$\left(\sum_{n=0}^{\infty} A_n\, e^{-nk_{CS,int}t}\right) = \sum_{n=0}^{\infty}\left(\frac{\lambda^n}{n!}e^{-\lambda}\right)\left(e^{-nk_{CS,int}t}\right) = e^{\left(\lambda\left[e^{(-k_{CS,int}t)}-1\right]\right)} \quad (6)$$

In eq 6, the parameter A_n is the fraction of the ensemble that have n adsorbed V^{2+}. When A_n is substituted with $p(n,\lambda)$ from eq 3, the infinite sum of exponentials converges to the expression on the right-hand side of eq 6.[2,28,29] We fit the kinetic traces at 620 nm with eq 1, but replaced the simple exponential function for Rise 2 with the Poisson-derived expression in eq 6 (Figure 7A). In the Poisson-derived function, we fixed the value of λ to that which we calculated using eq 5. Using this procedure, we obtained a value of $(1.6 \pm 0.3) \times 10^{10}$ s^{-1} for $k_{CS,int}$, averaged over all values of λ. Figure 7B shows that the value for $k_{CS,int}$ is constant with λ for all samples when using the Poisson-derived fit function, as we expect because the increase in observed PET dynamics for samples with higher concentrations of V^{2+} is accounted for entirely by λ.

The time dependence of the B1 feature includes the PET dynamics and the multiexponential decays of the "free" QDs (those without adsorbed V^{2+}) and is therefore more complicated than the 620 nm feature. We first fit the kinetic trace for B1 for free QDs with a sum of four simple exponential terms. Four exponential components are required to yield a symmetric scattering of residuals around the zero line for QDs with their native ligands (see the Supporting Information). When fitting the kinetic traces for samples with added V^{2+}, we assumed that the distributed dynamics of PET would be present in addition to the dynamics of the free QDs. We therefore used a sum of five terms, four simple exponentials and the Poisson-derived function in eq 6, and fixed the time constants for the four exponentials to those extracted from the fit of the free QD sample (we allowed the amplitudes of those components to float). As with our fits of the 620 nm feature, we fixed the value of λ in the Poisson-derived term (eq 6) of the fit function to the value we calculate from K_a. We find $k_{cs,int}$ to be $1.8 \pm 0.9 \times 10^{10}$ s^{-1} when fitting the B1 feature; this rate constant agrees with that we determined by fitting the V^+ feature at 620 nm. The Supporting Information contains comparisons of the kinetics of B1 and those of $V^{+\bullet}$.

For the CdS QD$-V^{2+}$ system, determining λ using the analysis of the bleach amplitude is critical for fitting the kinetic traces for B1 and $V^{+\bullet}$. If we do not fix λ in eq 6 when fitting our kinetic traces, we obtain unstable and unphysical values of λ and $k_{CS,int}$ from the fits of the 620-nm feature and the B1 feature; that is, we cannot extract statistically significant solutions for both λ and $k_{CS,int}$ from the kinetic data alone. In this case, therefore, analysis of the bleach amplitude facilitates determination of $k_{CS,int}$.

The Poisson-Derived Fit Function Is Well-Approximated by a Single Exponential Function for This System. We mentioned previously that the PET dynamics are adequately fit by a Poisson-derived function and a simple exponential (see the Supporting Information for a comparison). This simple exponential is a good approximation for the Poisson-derived fit function at short times;[45] for instance, given our estimated value of $k_{CS,int}$, the product $k_{CS,int}t$ at t = 10 ps is ~0.2, and the difference between the simple exponential $e^{(\lambda k_{CS,int}t)}$ and the Poisson-derived function in eq 6 is ~7% for $\lambda = 3$.

CONCLUSION

We have presented a method to determine λ, the mean number of redox-active ligands adsorbed to a QD in PET-active configurations, within an ensemble of QD$-$ligand complexes. Knowing the value of λ enables determination of the intrinsic rate of photoinduced electron transfer, $k_{CS,int}$, for a single CdS QD$-V^{2+}$ donor$-$acceptor pair, and the CdS QD$-V^{2+}$ adsorption constant, K_a. By simultaneously analyzing the magnitude of

the ground state bleach of the QD and the dynamics of the $V^{+\bullet}$ and B1 features as a function of added V^{2+}, we determined a value of $k_{CS,int} \sim 1.7 \pm 0.7 \times 10^{10}\ s^{-1}$ (Figure 7) and a value of $K_a = 4.4 \times 10^4\ M^{-1}$ (Figure 6). This work demonstrates the use of transient absorption to simultaneously investigate the PET process of a single QD−ligand couple and quantify the affinity of the ligand for the QD surface under the conditions of the PET experiment.

Our method does not directly provide information about the structure of the QD−V^{2+} interface; in calculating λ and K_a, we define an "adsorbed" V^{2+} as one that is in proper proximity and orientation to participate in the electron transfer process. Using this methodology, however, we can use the redox-active moiety as a probe of the binding process and determine the effects of the structure and composition of the ligand headgroup, the length of the linker between donor (QD) and acceptor (ligand), the size of the QD, and the presence of competing ligands on K_a and $k_{CS,int}$. Our method allows us to deconvolute the contributions of the adsorption constant and intrinsic charge transfer rate to the observed rate constant, and this capability will be extremely powerful in understanding the heterogeneous charge transfer process.

■ ASSOCIATED CONTENT

Supporting Information. Experimental details, characterization of CdS QDs, acetonitrile control experiments, dynamics of QD shelf formation, CV of V^{2+}, calculation of QD conduction and valence band edges, global analysis of 620 nm photoinduced absorption for high concentrations of V^{2+}, changes in $k_{CS,obs}$ per V^{2+} added, calculation of number of surface sites per QD, comparisons of data fit with Poisson-derived fit functions and basic-exponential fit functions, comparison of kinetics obtained at the B1 feature to those obtained at the $V^{+\bullet}$ feature, description of sources of error in calculating K_a, concentration dependence of K_a, and Figures S1−S15. This material is available free of charge via the Internet at http://pubs.acs.org.

■ AUTHOR INFORMATION

Corresponding Author
e-weiss@northwestern.edu

■ ACKNOWLEDGMENT

This material is based upon work supported under a NSF Graduate Research Fellowship (A.J.M.-C.), and by the DOE through the Office of Science Early Career Research Award (DE-SC0003998) to E.A.W.

■ REFERENCES

(1) Boulesbaa, A.; Issac, A.; Stockwell, D.; Huang, Z.; Huang, J.; Guo, J.; Lian, T. *J. Am. Chem. Soc.* **2007**, *129*, 15132–15133.
(2) Huang, J. E.; Huang, Z. Q.; Jin, S. Y.; Lian, T. Q. *J. Phys. Chem. C* **2008**, *112*, 19734–19738.
(3) Issac, A.; Jin, S. Y.; Lian, T. Q. *J. Am. Chem. Soc.* **2008**, *130*, 11280–11281.
(4) Boulesbaa, A.; Huang, Z.; Wu, D.; Lian, T. *J. Phys. Chem. C* **2010**, *114*, 962–969.
(5) Sharma, S. N.; Pillai, Z. S.; Kamat, P. V. *J. Phys. Chem. B* **2003**, *107*, 10088–10093.
(6) Klimov, V. I.; Mikhailovsky, A. A.; McBranch, D. W.; Leatherdale, C. A.; Bawendi, M. G. *Phys. Rev. B* **2000**, *61*, 13349–13352.
(7) Huang, J.; Huang, Z. Q.; Yang, Y.; Zhu, H. M.; Lian, T. Q. *J. Am. Chem. Soc.* **2010**, *132*, 4858–4864.
(8) Ramsden, J. J.; Gratzel, M. *Chem. Phys. Lett.* **1986**, *132*, 269–272.
(9) Serpone, N.; Sharma, D. K.; Jamieson, M. A.; Gratzel, M.; Ramsden, J. J. *J. Phys. Chem. Lett.* **1985**, *115*, 473–476.
(10) Matsumoto, H.; Uchida, H.; Matsunaga, T.; Tanaka, K.; Sakata, T.; Mori, H.; Yoneyama, H. *J. Phys. Chem.* **1994**, *98*, 11549–11556.
(11) Shallcross, R. C.; D'Ambruoso, G. D.; Pyun, J.; Armstrong, N. R. *J. Am. Chem. Soc.* **2010**, *132*, 2622–2632.
(12) Huang, J.; Stockwell, D.; Huang, Z. Q.; Mohler, D. L.; Lian, T. Q. *J. Am. Chem. Soc.* **2008**, *130*, 5632–5633.
(13) Kongkanand, A.; Tvrdy, K.; Takechi, K.; Kuno, M.; Kamat, P. V. *J. Am. Chem. Soc.* **2008**, *130*, 4007–4015.
(14) Robel, I.; Kuno, M.; Kamat, P. V. *J. Am. Chem. Soc.* **2007**, *129*, 4136–4137.
(15) Chakrapani, V.; Tvrdy, K.; Kamat, P. V. *J. Am. Chem. Soc.* **2010**, *132*, 1228–1229.
(16) Dibbell, R. S.; Watson, D. F. *J. Phys. Chem. C* **2009**, *113*, 3139–3149.
(17) Robel, I.; Subramanian, V.; Kuno, M.; Kamat, P. V. *J. Am. Chem. Soc.* **2006**, *128*, 2385–2393.
(18) Kamat, P. V. *J. Phys. Chem. C* **2008**, *112*, 18737–18753.
(19) Watson, D. F. *J. Phys. Chem. Lett.* **2010**, *1*, 2299–2309.
(20) Fritzinger, B.; Capek, R. K.; Lambert, K.; Martins, J. C.; Hens, Z. *J. Am. Chem. Soc.* **2010**, *132*, 10195–10201.
(21) Donakowski, M. D.; Godbe, J. M.; Sknepnek, R.; Knowles, K. E.; Olvera de la Cruz, M.; Weiss, E. A. *J. Phys. Chem. C* 2010, *114*, 22526–22534.
(22) Moreels, I.; Martins, J. C.; Hens, Z. *ChemPhysChem* **2006**, *7*, 1028–1031.
(23) Moreels, I.; Martins, J. C.; Hens, Z. *Sens. Actuators, B* **2007**, *126*, 283–288.
(24) Ji, X. H.; Copenhaver, D.; Sichmeller, C.; Peng, X. G. *J. Am. Chem. Soc.* **2008**, *130*, 5726–5735.
(25) Morris-Cohen, A. J.; Donakowski, M. D.; Knowles, K. E.; Weiss, E. A. *J. Phys. Chem. C* **2010**, *114*, 897–906.
(26) Katari, J. E. B.; Colvin, V. L.; Alivisatos, A. P. *J. Phys. Chem.* **1994**, *98*, 4109–4117.
(27) Kopping, J. T.; Patten, T. E. *J. Am. Chem. Soc.* **2008**, *130*, 5689–5698.
(28) Sadhu, S.; Tachiya, M.; Patra, A. *J. Phys. Chem. C* **2009**, *113*, 19488–19492.
(29) Tachiya, M. *J. Chem. Phys.* **1982**, *76*, 340–348.
(30) Logunov, S.; Green, T.; Marguet, S.; El-Sayed, M. A. *J. Phys. Chem. A* **1998**, *102*, 5652–5658.
(31) Matylitsky, V. V.; Dworak, L.; Breus, V. V.; Basche, T.; Wachtveitl, J. *J. Am. Chem. Soc.* **2009**, *131*, 2424–2425.
(32) Harris, C.; Kamat, P. V. *ACS Nano* **2009**, *3*, 682–690.
(33) Impellizzeri, S.; Monaco, S.; Yildiz, I.; Amelia, M.; Credi, A.; Raymo, F. i. M. *J. Phys. Chem. C* 2010, *114*, 7007–7013.
(34) Rossetti, R.; Beck, S. M.; Brus, L. E. *J. Am. Chem. Soc.* **1984**, *106*, 980–984.
(35) Rossetti, R.; Brus, L. E. *J. Phys. Chem.* **1986**, *90*, 558–560.
(36) Yildiz, I.; Raymo, F. M. *J. Mater. Chem.* **2006**, *16*, 1118–1120.
(37) Mezei, G.; Kampf, J. W.; Pecoraro, V. L. *New J. Chem.* **2007**, *31*, 439–446.
(38) McArthur, E. A.; Morris-Cohen, A. J.; Knowles, K. E.; Weiss, E. A. *J. Phys. Chem. B* 2010, *114*, 14514–14520.
(39) Yu, W. W.; Qu, L.; Guo, W.; Peng, X. *Chem. Mater.* **2003**, *15*, 2854–2860.
(40) Cooney, R. R.; Sewall, S. L.; Dias, E. A.; Sagar, D. M.; Anderson, K. E. H.; Kambhampati, P. *Phys. Rev. B* **2007**, *75*, 245311.
(41) Klimov, V. I.; Schwarz, C. J.; McBranch, D. W.; Leatherdale, C. A.; Bawendi, M. G. *Phys. Rev. B* **1999**, *60*, R2177–R2180.
(42) Klimov, V. I. *J. Phys. Chem. B* **2000**, *104*, 6112–6123.
(43) Haram, S. K.; Quinn, B. M.; Bard, A. J. *J. Am. Chem. Soc.* **2001**, *123*, 8860–8861.

(44) Song, N.; Zhu, H.; Jin, S.; Zhan, W.; Lian, T. *ACS Nano* **2011**, *5*, 613–621.
(45) Rodgers, M. A. J.; Da Silva E Wheeler, M. F. *Chem. Phys. Lett.* **1978**, *53*, 165–169.
(46) The R = 2.3 nm QDs show a low amplitude (~10%), single picosecond relaxation not observed in the other samples. This relaxation process does not affect our analysis of B1 because we compare B1 for each QD−V^{2+} sample to B1 for the QD-only sample at a set of time delays when the relaxation is complete and no other processes have begun.
(47) Attard, G.; Barnes, C. *Surfaces*; Oxford University Press: Oxford; New York, 1998.
(48) Bullen, C.; Mulvaney, P. *Langmuir* **2006**, *22*, 3007–3013.